Antarctic Science 4 (2): 241–248 (1992)

A microbarograph for internal gravity wave studies in Antarctica

P.S. ANDERSON[1], S.D. MOBBS[2], J.C. KING[1], I. McCONNELL[3] and J.M. REES[3]

[1]British Antarctic Survey, Natural Environmental Research Council, High Cross, Madingley Road, Cambridge CB3 0ET, UK
[2]Department of Applied Mathematical Studies, University of Leeds, Leeds LS2 9JT, UK
[3]Department of Applied and Computational Mathematics, University of Sheffield, Sheffield S10 2TN, UK

Abstract: Measurement of pressure fluctuations provides the best means of detecting atmospheric internal gravity waves at the Earth's surface. We have developed an instrument which is sufficiently sensitive to detect the small pressure fluctuations associated with such waves yet robust enough for deployment in an Antarctic environment. The instrument incorporates several novel features, both in its design and in the method of deployment used. A prototype instrument has been successfully deployed at the British Antarctic Survey's Halley Station during 1989. The design of an experiment using an array of six improved instruments is briefly described.

Received 9 July 1991, accepted 28 January 1992

Key words: Microbarograph, gravity waves, turbulence, meteorology

Introduction

Field studies of internal gravity waves in the lower troposphere (e.g. Merrill 1977, Hunt *et al.* 1985, Einaudi *et al.* 1989) have demonstrated that such waves are most readily detected by using sensitive microbarographs to measure the small wave induced fluctuations in surface pressure. The pressure fluctuations are generally no greater than 10 Pa in amplitude, with typical frequencies of 10^{-2}–10^{-4}Hz. Various instruments capable of measuring such fluctuations have been developed (e.g. Cook & Bedard 1971, Elliott 1972a).

In 1986, the British Antarctic Survey ran a programme of boundary layer measurements at Halley, Antarctica (King & Anderson 1988, King *et al.* 1989). Records from surface instruments (King *et al.* 1987, Rees & Mobbs 1988), radiosondes (Mobbs & Rees 1989) and SODAR (Culf 1989) revealed the presence of internal gravity waves in the stably-stratified lower troposphere. In particular, time series of the temperature difference between different levels in the surface layer showed clear wave-like variations when the surface inversion was strong. Although this is often the case during the polar winter, there are many occasions on which the surface inversion is destroyed by strong winds. Time series of near surface wind components are then dominated by turbulence and the temperature difference signal is weak. Nevertheless, the overlying troposphere remains stably stratified and gravity waves are still likely to be present.

In order to investigate gravity waves under the full range of meteorological conditions experienced at Halley, it was decided to deploy an array of microbarographs. In the Appendix, we demonstrate that pressure measurements are the best means of detecting gravity waves at the surface. This paper describes the development of a microbarograph suitable for use in regions of permanent snow cover and reports some measurements from a prototype instrument, which was deployed at Halley during 1989.

Design considerations

Our aim was to develop an instrument which would measure pressure fluctuations to a resolution of 0.1 Pa with a stability of 10 Pa hr^{-1} or better. Furthermore, the system had to operate at a site where there is permanent snowcover and where winter temperatures may fall to -50°C.

Few absolute pressure sensors are capable of measuring pressure fluctuations with a resolution of 0.1 Pa about a typical atmospheric pressure of 10^5 Pa. It is thus usual for microbarographs to use a differential pressure sensor to measure fluctuations in the pressure difference between a reference volume, held at a constant pressure close to mean atmospheric pressure, and the atmosphere. The pressure difference can be measured using a suitable commercially-available micromanometer.

Design and construction of the reference volume requires care. The container must be mechanically robust in order that atmospheric pressure fluctuations do not change its volume (and thus the internal pressure). Similarly, it must be kept at a constant temperature to avoid temperature-generated pressure fluctuations. In practice, it is impossible to achieve the required degree of temperature stability through active control. A temperature change of 0.01K produces a pressure change of about 3.7 Pa; quite large when compared with the desired system resolution of 0.1 Pa.

However, by constructing the reference volume of material with a large thermal capacity, insulating it and placing it inside a temperature-controlled enclosure, it is possible to keep the rate of change of reference volume temperature to less than 0.005 K hr^{-1}. The associated pressure changes are then small compared with the internal gravity wave signal, expected to be at least 10 Pa hr^{-1}.

Atmospheric pressure fluctuates by several kPa over periods upwards of one hour as a result of the passage of weather systems. The small pressure fluctuations associated with

https://doi.org/10.1017/S0954102092000373 Published online by Cambridge University Press

internal gravity waves will thus be superposed on these larger and slower pressure trends. In order to use a sensitive micromanometer (with a range of 100 Pa or less), it is necessary to keep the pressure of the reference volume close to the running mean atmospheric pressure. In a conventional microbarograph, this is achieved by venting the reference volume to the atmosphere via a calibrated leak with a suitable time constant. This acts as a high-pass filter, the characteristics of which can be calculated if the leak hydrodynamic resistance is known. In an instrument operating routinely below 0°C the very fine bore tubing required to construct a suitable leak could easily become blocked by ice. We thus adopted a different design: the reference volume is isolated from the atmosphere by an electrically-actuated valve. When the micromanometer has reached full range the valve is opened briefly to allow the reference volume pressure to return to the current atmospheric pressure. When the valve opens, the air in the reference volume expands (compresses) adiabatically, thus its temperature decreases (increases) and it is no longer in thermal equilibrium with the walls of the container. If the valve is closed immediately, the pressure in the volume will rise (fall) as the air temperature returns to the temperature of the container walls. The time for return to equilibrium is governed by the time scale of diffusion of heat from the container walls to the air. For a cylinder of radius 85 mm x height 110 mm, the time to reach 90% of the equilibrium pressure was of the order of 10^3 s. However, by packing the volume with wire wool, thus greatly increasing the area of material in contact with the air, this was reduced to a few tens of seconds. The output from the micromanometer is discontinuous at valve openings, but records can be matched up either side of the discontinuity when the data are processed and the response of the system is much simpler than that of a microbarograph which incorporates a leak. The valve dissipates 6 W while it is held open. If atmospheric pressure is changing very rapidly and there are a large number of valve openings in a short time, this can cause a measurable warming of the reference volume. However, under normal circumstances, the valve opens only infrequently and the heating is insignificant compared to other sources of temperature fluctuations.

The final part of the system which requires careful design is the means of venting the micromanometer to the atmosphere. The measurement head must be designed so that fluctuations in wind speed do not induce fluctuations in dynamic pressure at the head if true static pressure is to be measured. Several designs for static pressure measurement heads have been proposed (e.g. Elliott 1972a, Miskad 1976). An alternative approach, where only low-frequency fluctuations are of interest, is to construct a measurement head which averages fluctuations over an area (Bedard 1977). Since our instrument was to be used in an area of permanent snowcover, we decided to exploit the fact that snow is porous and atmospheric pressure fluctuations are known to penetrate to some depth.

Clarke *et al.* (1987) and Colbeck (1989) have investigated the movement of air through snow due to wind action by modelling the snow as a one-dimensional porous medium and then assuming a sinusoidal pressure perturbation on the snow/air boundary. Clarke & Waddington (1991) have investigated the three-dimensional problem of flows driven by pressure fluctuation over infinitely deep porous snow. We expect to observe plane travelling waves and thus only consider a two-dimensional problem, with the additional complication of a layer of non-porous ice underlying the snow.

Flow through a porous medium, such as snow, is best described by the differential form of D'arcy's law (Scheidegger, p.76, 1960),

$$\phi \frac{\partial \rho}{\partial t} = \nabla . \left[\frac{\rho K}{\mu} \nabla p \right] \tag{1}$$

where the small hydrostatic pressure gradient has been neglected. The pressure is denoted by p, ρ is the density of air and μ is dynamic molecular viscosity ($1{\cdot}789 \times 10^5$ kgm^{-1} s^{-1}). K is the permeability and ϕ the porosity.

Bateman (personal communication 1988) carried out a series of experiments to investigate the permeability of snow at a depth of about 0.5 m at Halley. By applying a steady pressure across a known size sample of snow, he derived a mean value for K of $3{\cdot}7 \times 10^{-8}$ m^2, close to the value of 1.0×10^{-8} m^2 used by Clarke *et al.* (1987). The porosity of snow, ϕ, may be evaluated using

$$\phi = \frac{\text{Volume of pores}}{\text{bulk volume}} = 1 - \frac{\text{bulk density}}{\text{density of ice}}. \tag{2}$$

By taking $\rho_{ice} = 9.17 \times 10^2$ kg m^{-3}, it was found that $0{\cdot}57 < \phi < 0{\cdot}62$ for these samples. Since snow density increases with depth, ϕ will decrease with increasing depth. Similarly, K will decrease with depth as the average pore size becomes smaller (Yen 1988). For simplicity, however, we follow previous workers and model the snow as a layer of uniform porosity and permeability overlying impermeable ice at some depth ℓ.

By assuming that air density is a linear function of pressure only, it is possible to eliminate the density terms from D'arcy's law. If pressure is then expressed as a sum of a mean term and a perturbation ($p = p_0 + p'$), D'arcy's law can be linearized to give

$$\frac{\partial p'}{\partial t} = D \nabla^2 p' \tag{3}$$

where the constant term $D = Kp_0/\mu\phi$. This linearized form of D'arcy's law assumes that temperature is constant: this approach is commonly used for gas flow through porous media (Colbeck 1989).

The snow layer was modelled as an infinitely long, two-dimensional strip of depth ℓ surmounting non-porous ice at $z = 0$. At the snow/ice boundary, the vertical flow vanishes. Using D'arcy's law in the form

$$\text{flow rate} = -\frac{K}{\mu} \nabla p, \tag{4}$$

(Scheidegger, p.74, 1960), we obtain the lower boundary condition $dp/dz = 0$. The upper boundary condition on the snow/air boundary was chosen to be a sinusoidal pressure

https://doi.org/10.1017/S0954102092000373 Published online by Cambridge University Press

perturbation of the form $p'(x,l,t) = P\sin(kx-\omega t)$, where k is the wavenumber, ω is the angular frequency and P is a constant amplitude parameter. From this, the phase speed, c, may be calculated from $c = \omega/k$. Since (3) is a linear equation, solutions can be summed and so used to approximate any wave shape on the surface using Fourier synthesis.

The non-transient part of the solution of Eq. (3) can be expressed as

$$\mathcal{P}(x,z,t) = \Re\left\{ iP\exp^{-i(kx-\omega t)}\frac{\cosh\sqrt{\left(\frac{i\omega}{D}+k^2\right)}z}{\cosh\sqrt{\left(\frac{i\omega}{D}+k^2\right)}\ell}\right\}, \quad (5)$$

where $\Re$ denotes the real part is to be taken. The small, transient part of the solution was ignored in this study as it is shortlived compared to the timescale of gravity waves. Eq. (5) was then written in the phase-amplitude form

$$\mathcal{P}(x,z,t) = PA(k,\omega,z)\sin\{kx-\omega t+\varepsilon(k,\omega,z)\}, \quad (6)$$

where A is the amplitude and ε the phase change due to the snow. Taking p_0 as 10^5 Pa and ϕ as 0·6 gives the value of D as approximately 340 $m^2 s^{-1}$. From this, the phase term, $\varepsilon(k,\omega,z)$, was calculated to be less than 5 degrees for all the likely values of frequency and depth of microbarograph to be encountered at Halley and for wavelengths greater than 20 m. If we use the substitution $k = \omega/c$ to eliminate k, the effect of the snow on the amplitude of the pressure signal can be expressed in terms of frequency and wave speed. This is shown in Fig. 1 for the case when the microbarograph is at a depth of 1 m. As the microbarograph was sampled every second, the maximum frequency considered is 0·5Hz. The amplitude reduction for phase speeds up to 10 ms^{-1} is illustrated. Rees & Mobbs (1988) showed that the waves in the surface layer at Halley had phase speeds less that 10 ms^{-1}. It can be seen that, at 1 m depth, the highest frequencies are attenuated by the snow, but lower

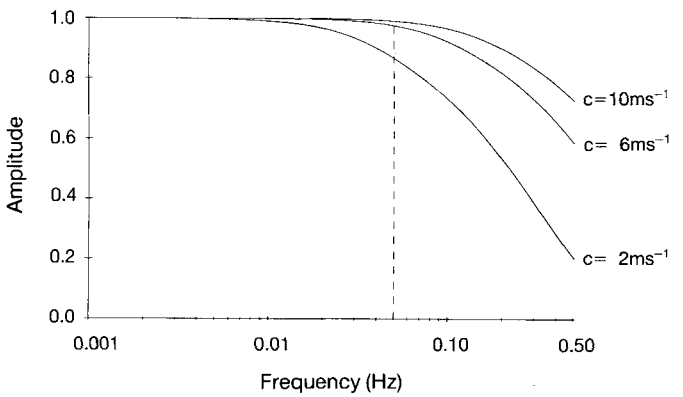


Fig. 1. Theoretical prediction of the variation of amplitude of a sinusoidal pressure signal with frequency for a microbarograph buried at a depth of 1m. Graphs are shown for phase speeds of 2, 6 and 10 ms .

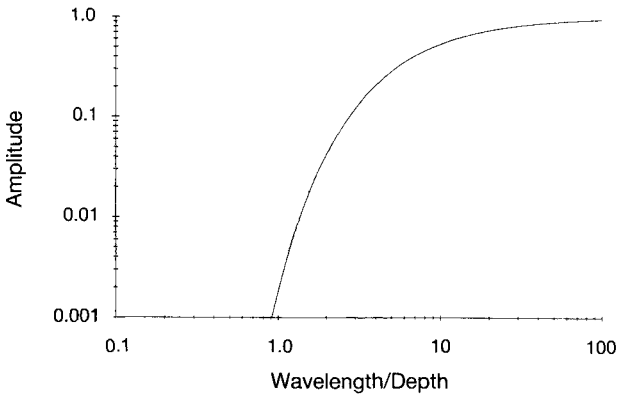


Fig. 2. Theoretical prediction of the variation of amplitude of a sinusoidal pressure signal of zero frequency against normalized wavelength.

frequencies (such as those typically associated with internal gravity waves) remain largely unaffected. The dashed line indicates the maximum frequency for data recorded as 10 second averages — current data sets are being recorded in this form.

From analysis of Eq. (5), it was found that wave number effects dominate frequency effects and that to a good approximation $A(k,\omega,z) = \exp(-kd)$, where d is the depth of the microbarograph below the surface. Relative amplitude then becomes a universal function of wavelength/depth (shown in Fig. 2), demonstrating clearly that the greatest reduction in amplitude will occur for short wavelengths (i.e. the turbulent part of the signal) or for large depths. Thus the microbarographs are able to record the pressure fluctuations associated with internal gravity waves, which have wavelengths of the order of hundreds of metres, while filtering out the fluctuations associated with turbulent eddies with typical scales measured in metres or tens of metres.

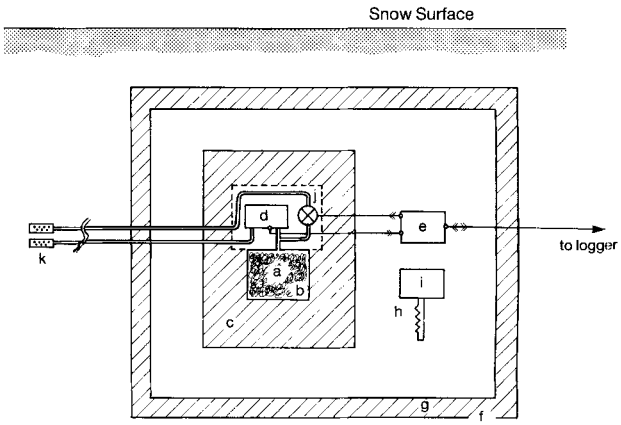


Fig. 3. A schematic diagram of the microbarograph. For legend, see text.

https://doi.org/10.1017/S0954102092000373 Published online by Cambridge University Press

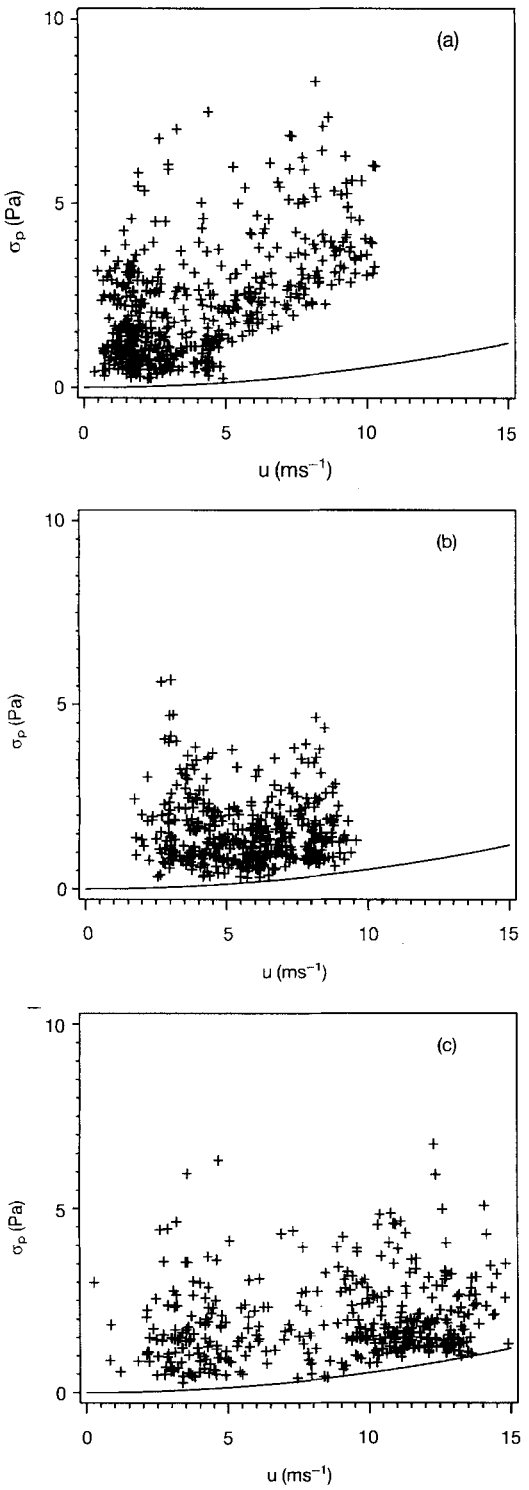


Fig. 4. 10-minute standard deviation of pressure as a function of wind speed for venting port depths of **a.** 0.05m, **b.** 0.5m and **c.** 1m. The solid line is the prediction of Eq. (9).

Description of the instrument

The construction of the instrument is shown schematically in Fig. 3. The reference volume vessel, (a), was constructed from stainless steel tubing 7 mm thick and enclosed a volume of 2 x 10^{-3} m^3 . It was packed with wire wool, (b), to help maintain thermal equilibrium between the air and vessel walls. The vessel was placed inside a 0.45 m cube of expanded polystyrene insulation, (c), to improve thermal stability.

A Furness Controls FCO40 micromanometer, (d), measured the pressure difference between the reference volume and the vent to the atmosphere. This sensor has a range of ± 100 Pa and produces an analogue voltage output which is linear to within 1% over the working range (manufacturer's calibration). The micromanometer output was sampled by an analogue to digital converter, (e), and was logged by a microcomputer. The logging system also controlled the venting valve, (j), which was of the "poppet" type. When the micromanometer reading reached ± 100 Pa, a signal was sent to open the valve until the reading dropped to ± 5 Pa.

The complete instrument was enclosed in a marine plywood box, (f) 1.04 m x 0.67m x 0.63m, lined with 50 mm expanded polystyrene insulation (g). Four heaters, (h), capable of dissipating a total of 580 W were connected to a proportional controller (Goulton/West 3400 series, i) and kept the temperature within the box at 5.0 ± 0.1 °C.

The box was designed to be buried beneath the snow surface providing further insulation from rapid changes in air temperature. A tube connected to the "atmospheric" side of the micromanometer ran through the box wall into a cavity in the snow which was kept open by a short length of perforated plastic pipe, (k). A similar tube was connected to the "atmospheric" side of the venting valve.

Performance of the prototype microbarograph

A prototype instrument was operated from January to July 1989 at Halley. In addition to the micromanometer output, the data logger also recorded absolute pressure (Vaisala DPA21 digital barometer, resolution of 10 Pa), microbarograph internal temperature and wind speed, direction and air temperature at 2 m. All were recorded continuously as 100 s averages with 10 s averages recorded for a period of 12 hours each week. Additionally, 10-minute values of the variance of the micromanometer reading, calculated from 1 s spot readings, were recorded continuously.

To assess the effect of the overlying snow on the pressure measurements, data were recorded for a number of days with the venting cavity placed at various depths beneath the snow surface. Pressure fluctuations in the snow are related to surface pressure fluctuations by a transfer function (Eq. 6) which depends on the depth of the measurement point and the wavenumber and frequency of the surface pressure disturbance.

Fig. 4 shows 10-minute values of σ_p, the standard deviation of 1-second pressure samples as measured by the microbarograph, plotted against wind speed at 2 m for three different measurement depths. Elliott (1972b) measured σ_p in the atmospheric surface layer and found:

$$\sigma_p \simeq 2.6\,\rho u_*^2 \qquad (7)$$

https://doi.org/10.1017/S0954102092000373 Published online by Cambridge University Press

where u_* is the friction velocity and ρ the air density. Under near-neutral stratification, u_* is related to the wind speed, $u(z)$ at height z by:

$$u_* = \frac{\kappa u(z)}{\ln(z/z_0)} \tag{8}$$

where κ is von Kármán's constant (~ 0.41) and z_0 is the roughness length. Strictly, a stability correction should be included in (8), but for conditions typical of Halley when $u > 5$ ms^{-1}, the error in u_* will be less than 10%. Using (7) and (8), and taking $z_0 = 0.0001$ m (King 1990) and $z = 2$ m (the height of the anemometer) gives:

$$\sigma_p \simeq 5.35 \times 10^{-3} u^2. \tag{9}$$

Fig. 4a shows that σ_p values are quite scattered when plotted against u, although, for a given u, there is a fairly well-defined minimum value of σ_p. Plots of the standard deviation of horizontal wind components as a function of windspeed also exhibit a well-defined minimum (King 1990). The solid line on Fig. 4a is the prediction of Eq. (9) and it is clear that even the minimum values of σ_p are significantly larger than predicted.

The snow surface at Halley is not perfectly flat, but consists of sastrugi of a variety of sizes. Colbeck (1989) considers steady wind flow over such a surface and demonstrates that this will generate steady pressure gradients within the snow. Furthermore, variations in wind speed will generate dynamical pressure fluctuations in addition to those associated with boundary layer turbulence. These pressure fluctuations will be of the order of the variations in the stagnation pressure, $\sigma_{ps} = \rho\, u(h)\sigma_u$ where $u(h)$ is the wind speed at a typical sastrugi height, h and σ_u is the standard deviation of wind speed. Under near-neutral conditions,

$$u(h) = \frac{u_*}{\kappa} \ln\left(\frac{h}{z_0}\right). \tag{10}$$

King (1990) measured $\sigma_u \simeq 2.2u_*$ hence

$$\frac{\sigma_{ps}}{\sigma_p} \simeq \frac{0.85}{\kappa} \ln\left(\frac{h}{z_0}\right). \tag{11}$$

At Halley, h is typically 0.1 m, hence $\sigma_{ps}/\sigma_p \simeq 15$. This simple order-of-magnitude calculation thus suggests that the pressure fluctuations observed just under the snow surface are likely to be substantially greater than those associated with boundary layer turbulence alone.

At 0.5 m depth (Fig. 4b), the dependence of σ_p on wind speed appears to be substantially reduced. The horizontal scale of the sastrugi is typically a few metres and Fig. 2 predicts an order of magnitude reduction for wavelengths of about 1.5 m at this depth. The behaviour at 1 m depth (Fig. 4c) is similar. It would thus appear that by making pressure measurements below the snow surface, it is possible to filter out pressure fluctuations caused by the interaction of wind with snow surface topography. The large scattered values of σ_p seen at all depths are probably associated with long-wavelength structures, such as internal gravity waves. These would not be expected to scale with u_* and will not be so strongly attenuated with depth.

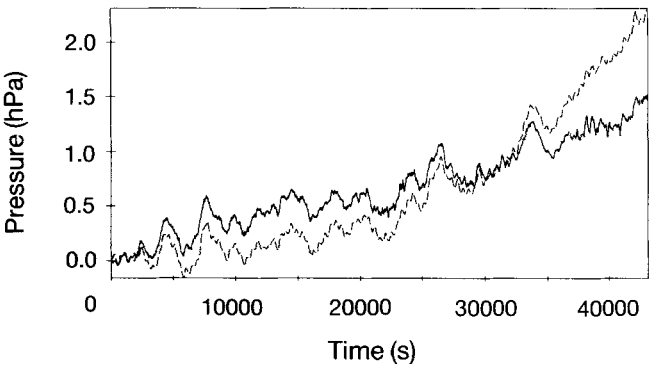


Fig. 5. Typical microbarograph (solid line) and absolute pressure sensor (broken line) traces.

A typical section of the microbarograph record, together with the absolute pressure record, is shown in Fig. 5. The absolute pressure sensor only has a resolution of 0.1 hPa and has thus been smoothed using a 30-point (i.e. 300 s) moving average. It would appear that the microbarograph consistently underestimates the magnitude of long-term pressure changes. Such consistent behaviour is more likely to be due to leaks in the system than temperature drift. It is possible to correct for the effects of leaks by making the assumption that the rate of pressure change inside the reference volume is proportional to the pressure difference between the reference volume and the exterior. Mathematically, this can be expressed as

$$\frac{d}{dt}\{(p_b - p_0) - \pi\} = r\pi \tag{12}$$

where p_b is the absolute pressure from a digital barometer, p_0 is the absolute atmospheric pressure when the valve opens, π is the microbarograph reading and r is the constant of proportionality which represents the magnitude of the leak. From this, an estimate of r was made by fitting a least-squares straight line through a graph of $d/dt\{(p_b - p_0) - \pi\}$ against π. The corrected pressure, p_c, was then calculated from

$$p_c = \pi + r\int_{t_0}^{t} (p_b(s) - p_0)e^{r(s-t)}ds \tag{13}$$

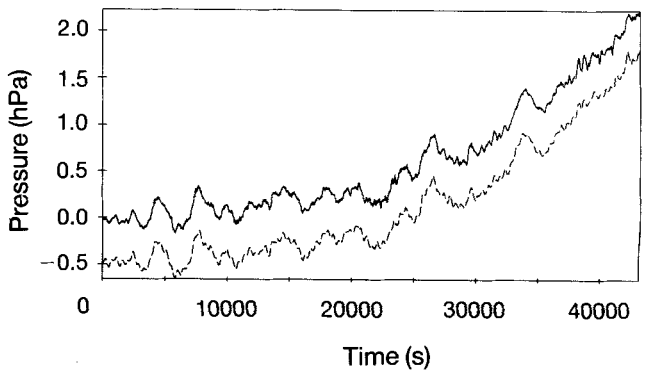


Fig. 6. As Fig. 5, but following correction of the microbarograph signal for the effects of the leak. The two signals have been displaced by an arbitrary 0.5 hPa for clarity.

https://doi.org/10.1017/S0954102092000373 Published online by Cambridge University Press

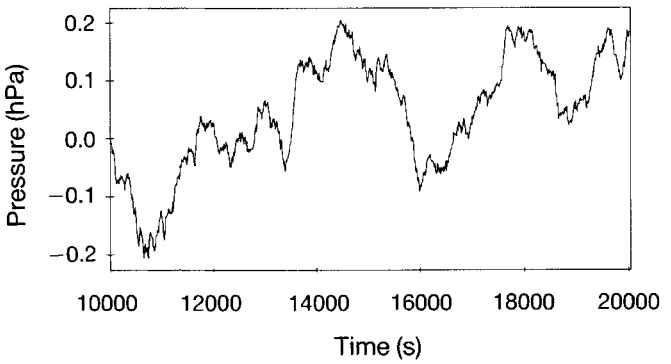


Fig. 7. A detailed section of the microbarograph record in Fig. 6 showing the wave activity.

where t_0 is the time at which the valve has just closed and the internal and external pressures of the reference volume agree. The corrected microbarograph record from Fig. 5 is shown in Fig. 6. A detailed section of the microbarograph record is shown in Fig. 7, exhibiting gravity wave signatures on a variety of time scales.

Further developments

An array of six microbarographs was deployed at Halley in January 1991. The design of these instruments is similar to that of the prototype described in this paper, but careful attention to the pipework connecting the reference volume and micromanometer and use of a "plunger"-type venting valve has reduced leakage to an acceptable level.

The instruments were set out in a triangular array which was designed to resolve gravity waves with wavelengths between 200m and 3500m. The design of the array and some preliminary results are discussed by McConnell *et al.* (1991).

Conclusion

We have demonstrated that it is possible to build a microbarograph with sufficient sensitivity and stability for studies of tropospheric internal gravity waves in the Antarctic. By measuring pressure fluctuations beneath the snow surface, it is possible to average out the signal due to small-scale turbulence while retaining that due to larger scale motions.

Acknowledgements

In designing this instrument, we benefitted from many helpful discussions with A.J. Bedard, A.J. Thorpe, A. Ibbetson and A.H.A. Samah. A. Tait maintained the prototype instrument at Halley during 1989. The measurements of snow porosity were carried out by A.E. Bateman. Reference volumes for the instruments were manufactured by the workshop staff of the Physics Department, University of Leeds. I.McC. is grateful to the Science and Engineering Research Council for provision of a CASE research studentship at the University of Sheffield and the British Antarctic Survey.

Disclaimer

The manufacturers of individual components of the microbarograph are named for the convenience of the reader. This should not be taken to imply endorsement, either by the authors or the British Antarctic Survey, of these products or to exclude the possibility that other products may be equally suitable for the purpose described.

References

BEDARD, A.J., JR. 1977. The D-C pressure summator: theoretical operation, experimental tests and possible practical uses. *Fluidics Quarterly*, **9**, 26–51.

CLARKE, G.K.C., FISHER, D.A. & WADDINGTON, E.D. 1987. Wind pumping: A potentially significant heat source in ice sheets. *In* WADDINGTON, E.D. & WALDER, J.S., *eds. The Physical Basis of Ice Sheet Modelling* (IAHS Publication No. 170). Wallingford: IAHS Press, 169-180.

CLARKE, G.K.C. & WADDINGTON, E.D. (1991). A three-dimensional theory of wind pumping. *Journal of Glaciology*, **37**, 89-96.

COLBECK, S.C. 1989. Air movement in snow due to wind pumping. *Journal of Glaciology*, **35**, 209-213.

COOK, R.K. & BEDARD, A.J.JR. 1971. On the measurement of infrasound. *Geophysical Journal of the Royal Astronomical Society*, **26**, 5-11.

CULF, A.D. 1989. Acoustic sounding of the atmospheric boundary layer at Halley, Antarctica. *Antarctic Science*, **1**, 363-372.

EINAUDI, F., BEDARD A.J. & FINNIGAN J.J. 1989. A climatology of gravity waves and other coherent disturbances at the Boulder Atmospheric Observatory during March - April 1984. *Journal of the Atmospheric Sciences*, **46**, 303-329.

ELLIOTT, J.A. 1972a. Instrumentation for measuring static pressure fluctuations within the atmospheric boundary layer. *Boundary-Layer Meteorology*, **2**, 476-495.

ELLIOTT, J.A. 1972b. Microscale pressure fluctuations measured within the lower atmospheric boundary layer. *Journal of Fluid Mechanics*, **53**, 351-383.

HOLTON, J.R. 1979. *An introduction to dynamical meteorology*. New York: Academic Press, 391 pp.

HUNT, J.C.R., KAIMAL, J.C. & GAYNOR, J.E. 1985. Some observations of turbulence structure in stable layers. *Quarterly Journal of the Royal Meteorological Society*, **111**, 793-815.

KING, J.C. 1990. Some measurements of turbulence over an antarctic ice shelf. *Quarterly Journal of the Royal Meteorological Society*, **116**, 379-400.

KING, J.C. & ANDERSON, P.S. 1988. Installation and performance of the STABLE instrumentation at Halley. *British Antarctic Survey Bulletin*, No. 79, 65-77.

KING, J.C., MOBBS, S.D., DARBY, M.S. & REES, J.M. 1987. Observations of an internal gravity wave in the lower troposphere at Halley, Antarctica. *Boundary-Layer Meteorology*, **39**, 1-13.

KING, J.C., MOBBS, S.D., REES, J.M. ANDERSON, P.S. & CULF, A.D. 1989. The Stable Antarctic Boundary Layer Experiment at Halley Station, *Weather*, **44**, 398-405.

MCCONNELL, I., REES. J.M., KING, J.C. & ANDERSON, P.S. 1991. Observations of internal gravity waves in the Antarctic boundary layer using a microbarograph array. *Preprint volume, 8th Conference on Atmospheric and Oceanic Waves and Stability*. Boston: American Meteorological Society, 332-335.

MERRILL, J.T. 1977. Observational and theoretical study of shear instability in the air flow near the ground. *Journal of the Atmospheric Sciences*, **34**, 911-921.

https://doi.org/10.1017/S0954102092000373 Published online by Cambridge University Press

MISKAD, R.W. 1976. An omni-directional static pressure probe. *Journal of Applied Meteorology*, **15**, 1215-1225.

MOBBS, S.D. & DARBY, M.S. 1989. A general method for the linear stability analysis of stratified shear flow. *Quarterly Journal of the Royal Meteorological Society*, **115**, 915-939.

MOBBS, S.D. & REES, J.M. 1989. Studies of atmospheric internal gravity waves at Halley Station, Antarctica, using radiosondes. *Antarctic Science*, **1**, 65-75.

REES, J.M. & MOBBS, S.D. 1988. Studies of internal gravity waves at Halley Base, Antarctica using wind observations. *Quarterly Journal of the Royal Meteorological Society*, **114**, 939-966.

SCHEIDEGGER, A.E. 1960. *The Physics of Flow through Porous Media*. Toronto: University of Toronto Press, 1-313.

YEN, Y-C, 1988. *On the pressure drop through a uniform snow layer*. (CRREL Report 88-14). Hanover, N.H.: U.S. Army Cold Regions Research and Engineering Laboratory.

Appendix: The surface pressure signal of internal gravity waves

The essential properties may be illustrated using the Boussinesq equations of motion linearized about a horizontal mean flow. This is a good approximation for atmospheric internal gravity waves with a vertical scale much less than the scale height (see e.g. Holton 1979). Consider first those waves for which the angular frequency, in a frame of reference moving with the mean flow, is much less than the inertial frequency. In this case we may neglect the Coriolis force and the equations are

$$\frac{\partial u'}{\partial t} + \overline{u}\frac{\partial u'}{\partial x} + w'\frac{\partial \overline{u}}{\partial z} = -\frac{\partial}{\partial x}\left(\frac{p'}{\rho_0}\right), \qquad (A1)$$

$$\frac{\partial w'}{\partial t} + \overline{u}\frac{\partial w'}{\partial x} = -\frac{\partial}{\partial z}\left(\frac{p'}{\rho_0}\right) + b', \qquad (A2)$$

$$\frac{\partial b'}{\partial t} + \overline{u}\frac{\partial b'}{\partial x} + N^2 w' = 0 \qquad (A3)$$

and

$$\frac{\partial u'}{\partial x} + \frac{\partial w'}{\partial z} = 0. \qquad (A4)$$

Here, y derivatives have been eliminated by choosing to examine plane waves and choosing x to be the direction of propagation. Mean quantities are denoted by an overbar and perturbations to the mean by a prime. u and w are the horizontal and vertical velocity components, p is pressure and $b'=-g\rho'/\rho_0$ is the buoyancy acceleration. ρ_0 is the basic state density which varies slowly with height and g is the acceleration due to gravity. N is the Brunt-Väisälä frequency which for simplicity we shall assume to be constant.

Plane wave solutions exist of the form

$$\left(u', w', \frac{p'}{\rho_0}, b'\right) = \left(\hat{u}(z), \hat{w}(z), \hat{P}(z), \hat{b}(z)\right) e^{i(kx-\omega t)} \qquad (A5)$$

where k is the horizontal wavenumber and w is the angular frequency. Substituting this into Eq. (A1)–(A4) and introducing the intrinsic frequency $\hat{\omega}=\omega-uk$ gives

$$-i\hat{\omega}\hat{u} + \hat{w}\frac{d\overline{u}}{dz} = -ik\hat{P}, \qquad (A6)$$

$$-i\hat{\omega}\hat{w} = -\frac{d\hat{P}}{dz} + \hat{b}, \qquad (A7)$$

$$-i\hat{\omega}\hat{b} + N^2\hat{w} = 0 \qquad (A8)$$

and

$$ik\hat{u} + \frac{d\hat{w}}{dz} = 0. \qquad (A9)$$

Eliminating $\hat{u}$, $\hat{P}$ and $\hat{b}$ gives the familiar Taylor-Goldstein Equation:

$$\frac{d^2\hat{w}}{dz^2} + \left[\left(\frac{N^2}{\hat{\omega}^2} - 1\right)k^2 + \frac{k}{\hat{\omega}}\frac{d^2\overline{u}}{dz^2}\right]\hat{w} = 0. \qquad (A10)$$

The other amplitudes are related to $\hat{w}$ via

$$\frac{d\hat{w}}{dz} = -ik\hat{u}, \qquad (A11)$$

$$\hat{P} = \frac{i\hat{\omega}}{k^2}\frac{d\hat{w}}{dz} + \frac{i}{k}\frac{d\overline{u}}{dz}\hat{w}, \qquad (A12)$$

and

$$\hat{b} = -\frac{iN^2}{\hat{\omega}}\hat{w}. \qquad (A13)$$

Consider first the simple case of zero shear. Now internal gravity waves observed near the surface are likely to have a modal structure in the vertical, because either they will be trapped near the surface, or, in the case of higher level sources, the downward propagating waves will reflect at the surface. Since w must vanish at the surface $z=0$, it is appropriate to take $\hat{w} \sim \sin mz$. By virtue of Eq. (A11), we therefore choose

$$\hat{u} = A\cos mz \qquad (A14)$$

where A is a constant and then (A11)–(A13) (with $d\overline{u}/dz=0$) give

$$\hat{w} = -\frac{ikA}{m}\sin mz, \qquad (A15)$$

$$\hat{P} = \frac{\hat{\omega}}{k}A\cos mz \qquad (A16)$$

and

$$\hat{b} = -\frac{N^2 k}{\hat{\omega}m}A\sin mz. \qquad (A17)$$

It is clear that w' and b' have nodes at the surface whilst u' and

https://doi.org/10.1017/S0954102092000373 Published online by Cambridge University Press

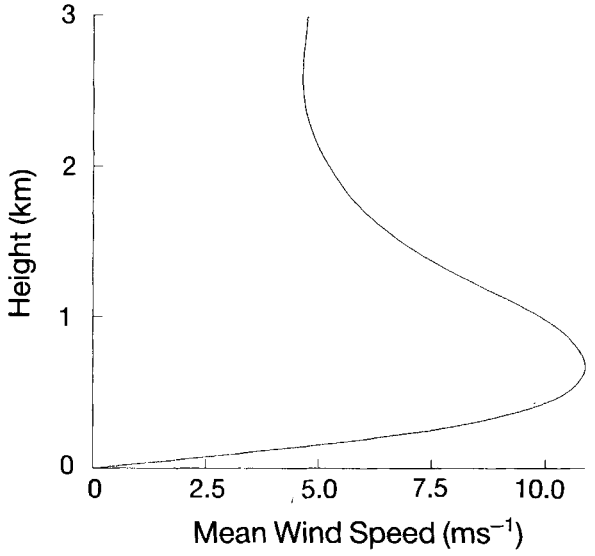


Fig. A1. A model mean flow profile used in the numerical solution of the Taylor-Goldstein Eq. (A10). This type of near surface jet profile is common at Halley.

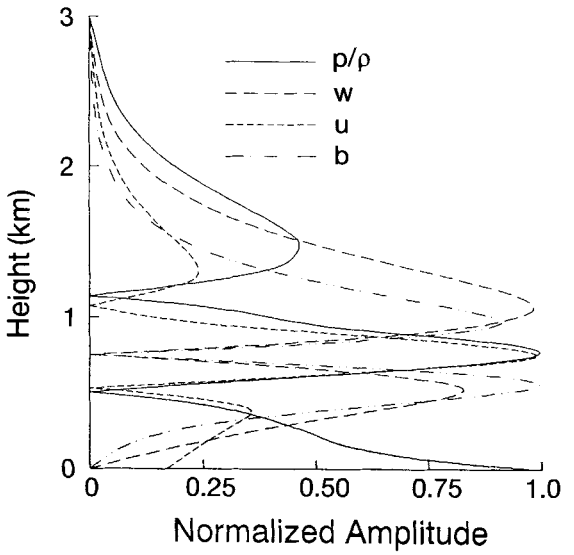


Fig. A2. The wave amplitude calculated by numerical solution of the Taylor Goldstein equation with the mean flow profile shown in Fig. A1. The horizontal wavelength is 1570m and there is a constant Brunt-Väisälä frequency of 0.02s^{-1}. The phase speed for the mode shown is 13.1ms^{-1}. Each profile is normalized to have a maximum value of unity.

p' have antinodes. Without the use of a tall mast, internal gravity waves should therefore be most clearly evident in the horizontal wind and pressure fields; the vertical velocity and buoyancy acceleration (or temperature) fields will demonstrate the wave activity less well. The wave signal in the horizontal wind will, additionally, be reduced and obscured by boundary layer effects. The turbulent boundary layer is likely to have less effect on the pressure.

The picture is changed quantitatively but not qualitatively by the presence of mean shear. As an illustration of this, a numerical solution of the Taylor-Goldstein Eq. (A10) is presented. Fig. A1 shows a mean velocity profile typical of the type observed at Halley which lead to trapping of internal gravity waves near the surface (Rees & Mobbs 1988). A numerical solution of (A10) with this wind profile and a constant Brunt-Väisälä frequency of 0.02s^{-1} is shown in Fig. A2. The solution presented is one of a wave trapped close to the surface, decaying evanescently above the jet in the mean wind. Mathematically, the problem is an eigenvalue problem for the angular frequency ω and the eigenfunction $\hat{w}$. Iterative solution, in order to find ω, is necessary (e.g. Mobbs & Darby 1989). The solution illustrated has a horizontal wavelength of 1570m and a phase speed of 13.1ms^{-1}. The amplitudes $|\hat{u}|$, $|\hat{w}|$, $|\hat{P}|$ and $|\hat{b}|$ are shown and each is normalized so as to have a maximum value of unity. It is quite clear that the pressure attains a large value at the surface whereas the vertical velocity and buoyancy acceleration have small values there. Due to the variation of the intrinsic frequency with height, even the horizontal velocity amplitude is substantially smaller at the surface than at higher levels.

The conclusions presented above are not changed qualitatively for the case of waves with intrinsic frequency similar to the inertial frequency, for which the Coriolis force is significant. The above analysis can be repeated for these inertio-gravity waves and we find that, for the case without shear, if

$$\hat{u} = A \cos mz \qquad (A18)$$

then

$$\hat{w} = -i\frac{k}{m}A \sin mz \approx -i\frac{\sqrt{\hat{\omega}^2 - f^2}}{N}A \sin mz, \qquad (A19)$$

$$\hat{P} = \frac{\hat{\omega}^2 - f^2}{\hat{\omega}k}A \cos mz \qquad (A20)$$

and

$$\hat{b} = -\frac{N^2 k}{\hat{\omega}m}A \sin mz = -\frac{N\sqrt{\hat{\omega}^2 - f^2}}{\hat{\omega}}A \sin mz \qquad (A21)$$

where f is the Coriolis parameter (i.e. f=2Ω sinϕ where ϕ is the latitude). Note that for these waves, $\hat{\omega}^2$ is always greater than f^2, but $\hat{\omega}^2$ and f^2 must be of similar magnitude for the Coriolis force to be significant. Both $|\hat{\omega}|$ and $|f|$ are both much less than typical values of N. Inertio-gravity waves typically have horizontal velocity perturbations of similar magnitude to internal gravity waves (a few ms^{-1}). It is clear from Eq. (A18)–(A21) that once again, the vertical velocity and buoyancy acceleration are small at the surface whereas the horizontal velocity and pressure are not. In the case of the vertical velocity, this effect is enhanced by the fact that ω is small everywhere since $|\hat{\omega}| << N$. Again, we conclude that pressure measurements are ideal for detecting the surface signature of these waves.

https://doi.org/10.1017/S0954102092000373 Published online by Cambridge University Press